energies

MDPI

Article

An Analysis of Decentralized Demand Response as Frequency Control Support under Critical Wind Power Oscillations

Jorge Villena [1,*], Antonio Vigueras-Rodríguez [2,†], Emilio Gómez-Lázaro [3,†], Juan Álvaro Fuentes-Moreno [4,†], Irene Muñoz-Benavente [4,†] and Ángel Molina-García [4,†]

Received: 4 September 2015 ; Accepted: 4 November 2015; Published: 13 November 2015
Academic Editor: Ying-Yi Hong

[1] CF Power Ltd., Calgary, AB T2M 3Y7, Canada
[2] Department of Civil Engineering, University of Cartagena, Cartagena 30203, Spain; avigueras.rodriguez@upct.es
[3] Renewable Energy Research Institute and DIEEAC/EDII-AB, Universidad de Castilla-La Mancha, Albacete 02071, Spain; emilio.gomez@uclm.es
[4] Department of Electrical Eng., Technical University of Cartagena, Cartagena 30202, Spain; juanalvaro.fuentes@upct.es (J.A.F.-M.); irene.munoz@upct.es (I.M.-B.); angel.molina@upct.es (A.M.-G.)
* Correspondence: jvillena@cfpowerltd.com; Tel.: +1-587-719-3947
† These authors contributed equally to this work.

Abstract: In power systems with high wind energy penetration, the conjunction of wind power fluctuations and power system inertia reduction can lead to large frequency excursions, where the operating reserves of conventional power generation may be insufficient to restore the power balance. With the aim of evaluating the demand-side contribution to frequency control, a complete process to determine critical wind oscillations in power systems with high wind penetration is discussed and described in this paper. This process implies thousands of wind power series simulations, which have been carried out through a validated offshore wind farm model. A large number of different conditions have been taken into account, such as frequency dead bands, the percentages of controllable demand and seasonal factor influence on controllable loads. Relevant results and statistics are also included in the paper.

Keywords: wind power generation; frequency control; load management; demand response

1. Introduction

The integration of intermittent renewable energy sources into power systems can be limited due to their disruptive effects on power quality and reliability. In the case of wind energy, the increasing penetration of this type of power generation may involve changes in power system design and management, such as grid reinforcements [1] and the necessity of studying its impact on grid frequency control [2,3]. In a power system, keeping a close balance between the generated and demanded power is an important operational requirement to maintain the grid frequency within a narrow interval around its nominal value [4]. Nowadays, grid frequency is controlled by conventional power plants driven by conventional generation sources. The main goal of this control is to keep the frequency within specified limits according to each country's grid code, addressing power imbalance exclusively by modifying the generated power, since demand is generally considered as not controllable. In this way, conventional generators are usually equipped with so-called primary and secondary control, which are part of this grid frequency control. Primary frequency control involves all actions performed locally at the generator to stabilize the system frequency after a power disturbance. These actions achieve a stable grid frequency, but different from its nominal value. The

goal of the secondary frequency control is then to maintain the power balance within a bigger area, not just locally, as well as to recover the system frequency to its nominal value. These frequency control mechanisms are mainly performed by conventional power plants. In recent years, the rapid development of wind turbine technology and increasing wind power penetration in the generation mix have resulted in a continuous reformulation of wind power requirements to be integrated with traditional generation sources. Some transmission system operators have unified requirements and connection rules for all production units, whether they are driven by conventional energy sources or not, which are very difficult for wind turbine producers and wind farm developers to fulfill [5]. Under such conditions, in regions where there is a high wind energy penetration and whose interconnections are weak, difficulties in maintaining the nominal frequency could arise if sufficiently large wind power fluctuations occur.

System inertia also plays an important role in the grid frequency control, limiting the rate of frequency change under power imbalances. The lower the system inertia, the higher the rate of frequency change when demand-side or supply-side variations appear. System inertia is directly related to the amount of synchronous generators in the power system. This inherent relation is not as obvious when dealing with wind turbine generators due to the electromechanical characteristics of the currently prevailing variable speed technologies, whose turbine speed is decoupled from the grid frequency [6]. The inertia contribution of wind turbines is much less than that of conventional power plants [6–8]. Actually, some variable speed wind turbines use back-to-back power electronic converters, which create an electrical decoupling between the machine and the grid, leading to an even lower participation of wind generation to the system stored kinetic energy.

Some authors suggest that this drawback can be compensated by an adequate implementation of the machine control. In [9,10], a power reserve is obtained following a power reference value lower than the maximum power, which can be extracted from the wind, thus decreasing the turbine power efficiency. A method to let variable-speed wind turbines emulate inertia and support primary frequency control using the kinetic energy stored in the rotating mass of the turbine blades is proposed in [11]. In [12], a power reserve is obtained with the help of pitch control when the wind generator works close to the rated power.

With the aim of reducing the impact of wind power fluctuations and wind turbines lower inertia contribution to grid frequency control, demand-side actions can also be considered: switching-off some loads has similar effects on a grid power imbalance as increasing in the supply-side, reducing the need for ramp up/down services provided by conventional generators [13]. However, demand-side actions have been usually contemplated only in emergency situations to save the power system, such as load shedding [14,15] actions or load curtailment [16] and considering a minimum level of aggregated load power.

In this context, different load shedding schemes that have been proposed take into account a certain frequency threshold, as well as a certain rate of change of frequency (ROCOF) [17–20]. This demand-side complementary control could significantly help in maintaining grid frequency, as some authors consider that 40% of residential appliances are compatible with the proposed load control strategies [21]. Due to the high penetration of cooling and heating loads, about 20 percent of the load in the U.S. comes from consumer appliances that cycle on and off and which could make a contribution to frequency control during the normal operation state [22]. In [23], the authors present a centralized management system focused on electric water heaters for areas with a high penetration of renewable energy sources, in order to smoothen the imbalances between generation and demand within the controlled area. In [24], the authors assess what real-time operation could be like with a significant amount of active frequency-sensitive fridge/freezer load for the national grid system in Great Britain. The advantages of a higher proportion of these types of loads when wind penetration increases are also discussed. In [25], a decentralized approach for using thermal controllable loads (TCL) for providing primary frequency response is shown. The authors argue that a two-way communication between these loads and the control center is not essential. They

thus propose a frequency-responsive load controller, allowing the loads to respond under frequency changes in a similar way as conventional generators do. They also show that, using this approach, the demand side can make a significant and reliable contribution to primary frequency control without affecting the customers' comfort. Recently, the authors have also discussed the effectiveness of demand-side participation in primary frequency control together with the action of auxiliary frequency control carried out by variable-speed wind turbines, focused on evaluating the potential of additional controls and the compatibility between those controls [26]. In [27], following a similar decentralized approach, TCLs are grouped according to their essentiality for the customer, and in the event of a frequency drop, each of them is switched off for a predefined time, which depends on the frequency deviation.

Considering previous contributions, this paper discusses and describes a complete process to determine realistic wind speed oscillations. This process is able to evaluate the contribution of the demand side to primary frequency control in power systems with high wind penetration, providing a wide range of realistic wind speed variations and allowing one to analyze the demand response as frequency-controlled reserves under critical circumstances. The rest of the paper is structured as follows: In Section 2, the different components of the power system model used in this study are described. The proposed methodology for critical wind power fluctuations is described in Section 3. Simulations and results are given in Section 4. Finally, conclusions are discussed in Section 5.

2. Power System Model

2.1. General Description

For frequency control study purposes, power systems are usually modeled according to the general scheme shown in Figure 1. As can be seen, all turbine generators are lumped into a single equivalent rotating mass (M), and similarly, all individual system loads are lumped into an equivalent load with an equivalent damping coefficient (D) [28]. Additionally, frequency deviations are used as feedback signals for primary and secondary frequency control.

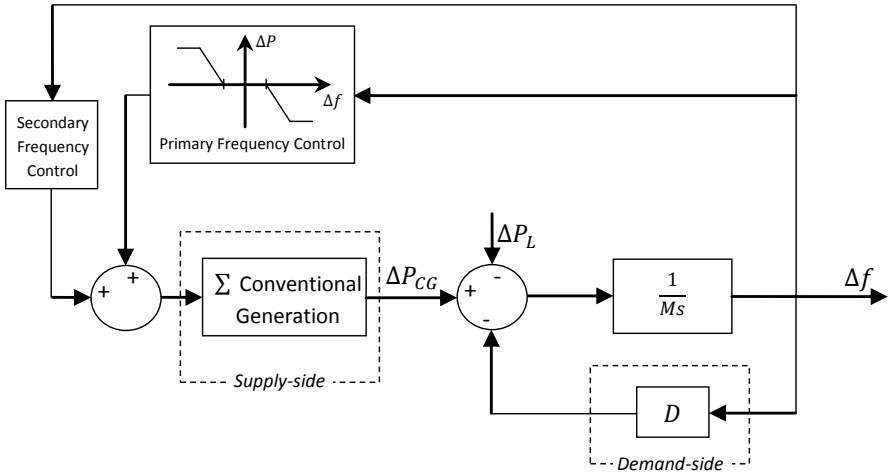

Figure 1. General scheme of a power system.

According to [28], the mathematical model of the power system can be expressed as:

$$\Delta P_{mec} - \Delta P_L = D'\Delta f + 2H\frac{d\Delta f}{dt} \quad (1)$$

In this equation, $\Delta P_{mec} - \Delta P_L$ represents the imbalance between power supply and demand, Δf is the consequent variation of the grid frequency; D' is the damping coefficient expressed in pu and H is the inertia constant, in seconds; with $M = 2H$. In this study; ΔP_L is not considered, so frequency

excursions are caused by typical fluctuations in wind power generation. Figure 2 shows the schematic block diagram of the power system model used in this work.

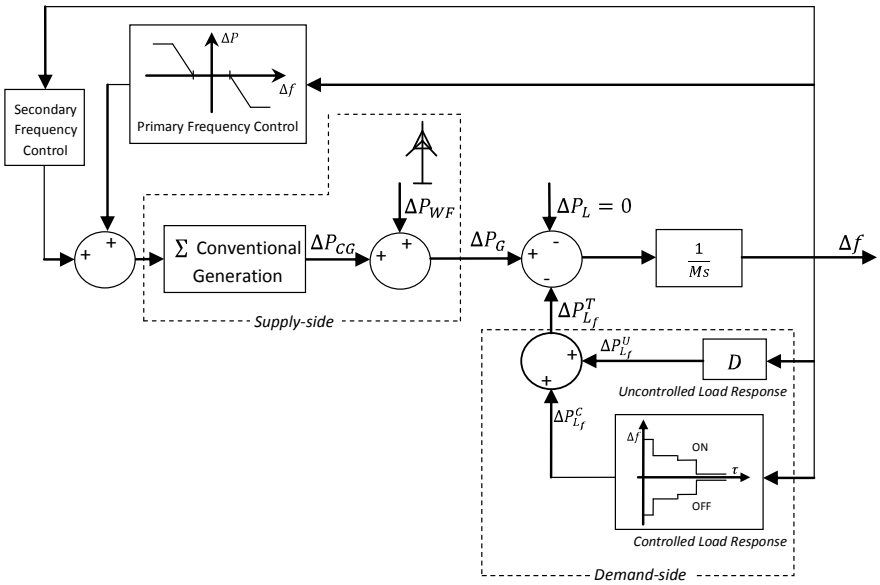

Figure 2. General scheme of the power system with the demand-side contribution to primary frequency control and wind power generation.

2.2. Supply-Side Model

The generation part of the power system model shown in Figure 2 consists of a thermal power plant and an offshore wind farm, which allows for simulating different energy mixes.

2.2.1. Conventional Generation

The conventional generation block shown in Figure 2 consists of a thermal power plant with a reheating system. The power plant model includes the transfer functions for the two main elements of the control loop: the primary energy-mechanical torque converter (governor) and the mechanical torque-electrical power converter (turbine), as detailed in [28,29]. The block diagram corresponding to this system is shown in Figure 3. The power plant is modeled to provide load-frequency control. The aim of the primary frequency control or speed governor is to change the primary energy input in order to maintain the generator's rotating speed as close as possible to the rated speed. The generator's rotating speed may change as a consequence of any modification in the power demanded by the customer side or by a rise or fall in the power produced by other generators. The speed governor response takes place within a few seconds, according to the speed-droop characteristic shown in Figure 3, in order to restore the active power balance. However, after the governor response, the grid frequency stabilizes, but differs from its nominal value. Secondary frequency control or automatic generation control (AGC) then takes place within one to several minutes to restore the power balance in a bigger area, not just locally, and to take the system frequency back to its nominal value. In this work, as only one generator models the controllable supply side, AGC is implemented through the loop shown in Figure 2, which consists of an integral control that aims to reduce the frequency error to zero. Limitations on slope and maximum power output variations are included for the generator, as well as a dead band (DB) to model the sensors sensibility and the precision of frequency measuring [30,31]. Changes in power from the supply side come solely from the wind farm power fluctuations, whilst the average demanded power remains constant during the simulations.

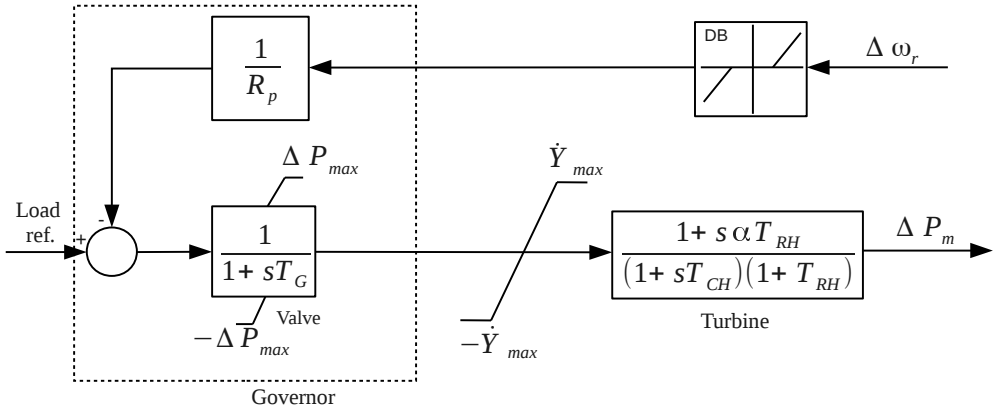

Figure 3. Model of the thermal plant.

2.2.2. Wind Power Generation

The wind power generation input in the supply side of Figure 2 consists of a wind power time series ($\Delta P_{WF}(t)$) obtained from an aggregated model of power fluctuations in an offshore wind farm (WF). The WF model was previously validated by comparing its results with real power fluctuations measured at the Nysted offshore wind farm. The WF model can be divided into two main blocks: a generator of spatially-averaged wind speed time series and an aggregated power curve that relates WF wind speed with WF power generation; see Figure 4. The first block takes the input to the simulator, which is the average wind speed upstream from the wind farm ($\overline{V_\infty}$), *i.e.*, far enough not to be affected by the wind farm, and outputs a spatially-averaged time series of the wind speed within the wind farm. The second block takes this wind speed and passes it through the wind farm model, which consists of an aggregated wind farm power curve, yielding the simulator output: a second 2-h series of wind farm power generation ($P_{WF}(t)$).

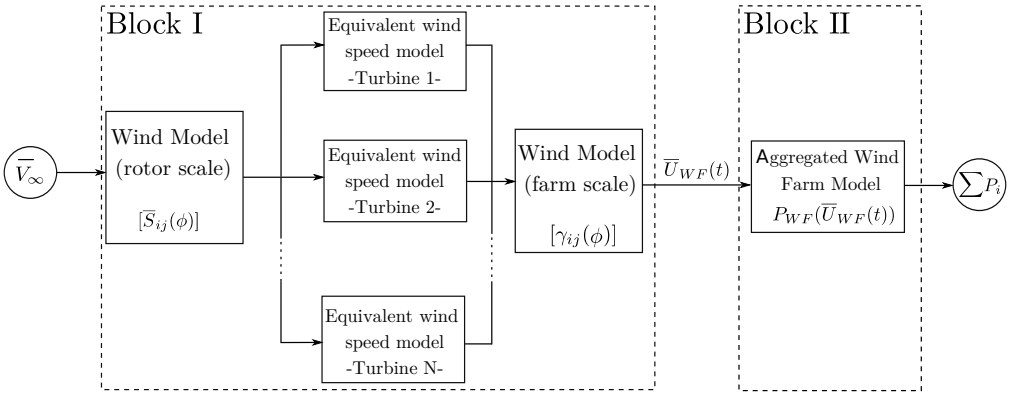

Figure 4. Wind farm power simulator scheme.

As mentioned in the previous paragraph, wind speed fluctuations within a wind farm can be modeled through spectral tools, like power spectral density (PSD) and spectral coherence. Such functions are defined in the frequency domain. In this section, frequency is represented as ϕ in order to avoid confusions with the electrical frequency, f.

Particularly, wind speed fluctuations in a single point are described by the following PSD ($S(\phi)$) function:

$$S(\phi) = \beta_{\mathrm{LF}}^2 \frac{\frac{z}{\overline{V}}}{\left(\frac{z\cdot\phi}{\overline{V}}\right)^{\frac{5}{3}} \cdot \left(1 + 100\frac{z\cdot\phi}{\overline{V}}\right)} + \sigma_V^2 \frac{2\frac{L_1}{\overline{V}}}{1 + 6\frac{L_1}{\overline{V}}\cdot\phi} \quad (2)$$

where ϕ is the frequency; z is the turbine hub height above sea level; $\overline{V}$ is the average wind speed within the wind farm and σ_V is its standard deviation. Finally, β_{LF} is an empirical parameter suggested by [9]. A numerical value of $\beta_{\mathrm{LF}} = 0.04\ \mathrm{ms}^{-1}$ is proposed by [32], based on experimental data from the Nysted and Horns Rev offshore wind farms.

Some quick variations of wind speed are directly smoothed at the rotor disk. Actually, wind turbines obtain their power from the wind speed within an area where part of these quick oscillations are not correlated. This issue is taken into account through the equivalent wind speed rotor model ($F_{\mathrm{EWS}}(\phi)$) suggested by [33]; see Figure 4. The equivalent wind speed, as shown in Figure 5, is the wind speed that, when applied uniformly on the entire rotor surface, produces the same aerodynamic torque as with the actual wind speed. Moreover, the spatial aggregation of wind turbines can contribute to smoothening part of the wind oscillations affecting individual WTs. This is taken into account by means of the spectral coherence model $\gamma_{\mathrm{i,j}}(\phi)$, which measures the relation of wind speed between two wind turbines (e.g., turbine numbers i and j). The coherence model implemented for this simulator is the one presented in [32].

Combining $S(\phi)$ and $\gamma_{\mathrm{i,j}}(\phi)$ as described in [34], the WF average wind speed PSD ($S_{\mathrm{av}}(\phi)$) can be obtained by:

$$S_{\mathrm{av}}(\phi) = \frac{1}{N^2}\left(\sum_{i=1}^{N}\sum_{j=1}^{i} 2\mathrm{Re}\left(\gamma_{\mathrm{i,j}}(\phi)\right)\right)\left(F_{\mathrm{EWS}}(\phi)\cdot S(\phi)\right) \quad (3)$$

being N the number of wind turbines in the wind farm and $\mathrm{Re}\left(\gamma_{\mathrm{i,j}}(\phi)\right)$ the real part of $\gamma_{\mathrm{i,j}}(\phi)$.

From the above PSD, $S_{\mathrm{av}}(\phi)$, time series of WF average wind speed are generated following the algorithm suggested in [32,35], whose scheme is shown in Figure 4. These wind speed series are converted into WF generated power series through an aggregated power curve, such as the one shown in Figure 6.

The power curve shown in Figure 6 in particular is an empirical curve measured at the Nysted offshore wind farm [36]. The curve is calculated by monitoring the total wind farm power output and the average wind speed within the wind farm, measured at the nacelle of each wind turbine. Usually, in order to calculate the power curve of a single wind turbine, the wind speed is measured ahead of the nacelle. The actual wind speed at the nacelle is slightly smaller. The wind speed shown in the figure is the average within the wind farm. Therefore, when the wind farm average wind speed is around 23 m/s, some wind turbines are already at their cut-out point (25 m/s) and automatically stop producing power. As wind speed rises, more wind turbines cut out, up to an average wind speed of around 27 m/s, at which all wind turbines are disconnected, hence the slope of the right part of the curve, which differs from the vertical shape of a single wind turbine power curve. Besides, it can be seen in the figure that the maximum power is below 1 pu. This is due to the effect of the wakes within the wind farm, especially when considering wind directions that are not optimal [37]. Thus, when the wind speed is around 15 m/s, the first row extracts the maximum power from the wind; the wind flowing to the second row, due to the turbulence, has less available energy, and so on. Overall, the total wind farm power is lower than 1 pu, although the wind speed is above the nominal speed. As wind speed increases, more rows will produce the maximum power, but the available power at the last rows will still drop below the nominal value. As wind speed goes above 23 m/s, the cut-out speed, the first rows (the higher the wind speed, the more rows will cut out) will automatically stop producing power, hence the slope of the right part of the curve, which differs from the vertical shape of a single wind turbine power curve.

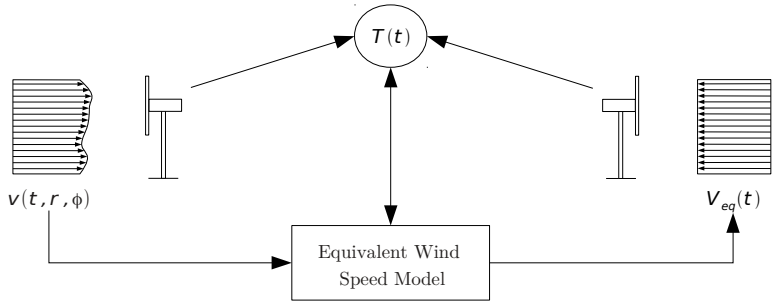

Figure 5. Scheme of the equivalent wind speed.

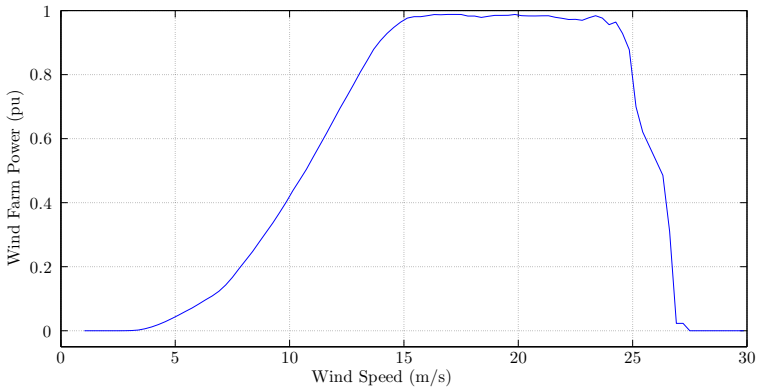

Figure 6. Aggregated wind farm power curve.

2.3. Demand-Side Model

The power demand is divided into two types of loads: uncontrollable and controllable loads. Uncontrollable loads are lumped into a single equivalent load, where the power consumption depends only on the system frequency changes through parameter D; see Figure 2. Controllable loads are modeled individually and involve those appliances with high thermal inertia mainly due to the following reasons: they comprise a significant portion of electricity consumption in the residential sector and their operation can be shifted in time without noticeable effects on consumers. Over 30% of the total electricity demand is consumed in households [38,39], of which more than 40% is compatible with the proposed forced connection/disconnection actions [21]. The number of controllable loads belonging to the residential sector is higher than the commercial sector. Moreover, their rated power is usually lower in comparison with the commercial sector. Thus, for the same amount of controlled power, a greater number of individual loads results in a smoother global response.

The load controller previously proposed in [25] is used to turn off (on) the controllable demand, which is assumed dependent on the grid frequency through parameter D. Actually, the influence of grid frequency excursions on the controllable power demand can be considered negligible in comparison with the forced disconnection (connection) commands set by the load controllers. These controllers consider not only the frequency deviation Δf, but also its evolution over time τ. In this way, each load controller has an associated Δf–τ profile that determines when the load starts contributing to the frequency control. As long as the frequency deviation does not exceed a certain threshold for a certain time, the load controller remains inactive, and the load maintains its normal operation demand. If the frequency deviation enters into the control region, the controller will switch off (on) the load, reducing (increasing) the power demand. Figure 7 shows the Δf–τ characteristics for different types of loads. Controllable loads have been grouped into three main categories according to the specific operating characteristics of each type of load and the patterns of use: fridges/freezers (Load Group I), air-conditioners/heat pumps (Load Group II) and electric

water heaters (Load Group III); see Table 2. These operating characteristics must be set in the load controller, and they define its behavior, *i.e.*, contingency response speed (given by t_{delay}), maximum off time and the minimum recovery time. A suitable configuration of these parameters allows us to preserve the minimum standards of customers' comfort and to consider mechanical and electrical load requirements. For example, randomly setting t_{delay} (assigning different values to each individual controlled load) avoids instantaneous and massive disconnections and, consequently, undesired frequency oscillations, therefore ensuring a smoother demand response. Moreover, the recovery time is required after forced disconnections (or connections) for the thermal variables to recover their ordinary values. Further information and a detailed description of the load controller algorithm can be found in [25].

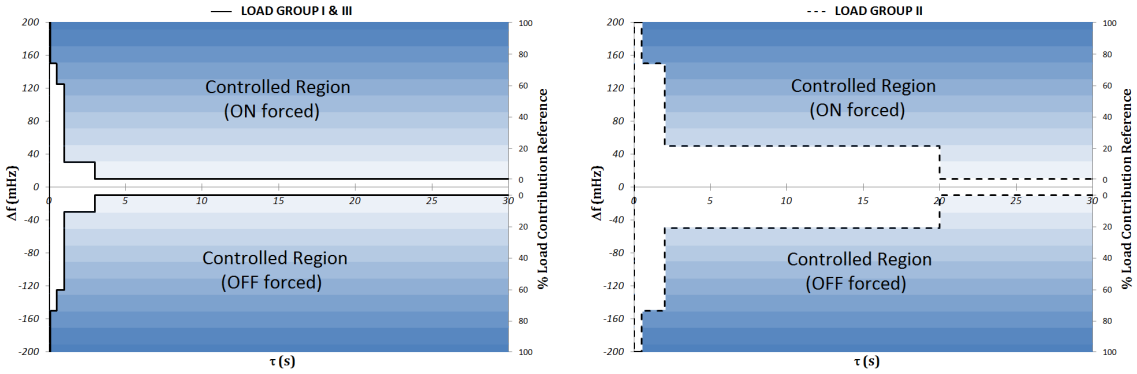

Figure 7. Frequency responsive load controller: Δf–τ characteristics. (**a**) Load Groups I and III; (**b**) Load Group II.

With the aim of providing a demand response that is proportional to the frequency excursion, controllable loads are called up to participate in the frequency control progressively depending on the depth of such an excursion; see Figure 7, the percentage of load contribution reference. Under a certain frequency event, the actual percentage of load contribution will depend on the connection status of each individual load according to its duty-cycle.

3. Simulation of Critical Wind Power Fluctuations

Realistic wind power series with high fluctuations are estimated with the aim of evaluating the wind power fluctuations' impact on the grid frequency. These series are determined as follows; see Figure 8.

- A set of 10,000 2-h series, with a one-second sample rate, of WF wind speed ($V_{WF}(t,j)$) is firstly estimated. The inputs to the wind farm model are an upstream 2-h average wind speed ($\overline{V}_j$) according to a Weibull probability distribution, as well as a spectral wind farm model [32,35,40].

  In this case, the wind is simulated considering a 506-MW offshore wind farm, with 10 rows with 22 wind turbines in each row.
- Realistic wind power data series ($P_{WF}(t,j)$) are obtained from $V_{WF}(t,j)$ through an aggregated wind farm power curve [36]. These series correspond to a global period of time of around 2.5 years, which is large enough for obtaining significant wind fluctuations.
- In order to characterize the power oscillations within the series, ramp power rates each of 2-min intervals are calculated ($P_{ramp}(n,j)$). This interval length is between the characteristic times of frequency control and wind power oscillations.
- Calculated ramp rates ($\forall j$ & n) are then sorted in descending order, obtaining the duration curve.

- From the stability point of view, the most critical cases are those where both wind power drops are steep, as well as the wind power share in the current mix of generation is high. Indeed, the ramp rate around the 99th-percentile with the highest wind power share is selected (n_{P99}), and the corresponding 2-h series where this drop happens is identified (j_{P99}) within the set of WF power series ($P_{WF}(t,j)$).
- A 10-min time interval around the n_{P99} event is selected to provide suitable frequency oscillations in the modeled power system $P_{WF_s}(t)$. Such a 10-min interval is highlighted in red color in Figure 9.
- Finally, wind power deviation (ΔP_{WF}) shown in Figure 2 is determined as the difference between $P_{WF}(t, j_{P_{99}})$ and the expected wind power within this time interval (P_{WF_0}),

$$\Delta P_{WF}(t) = P_{WF}(t, j_{P_{99}}) - P_{WF_0}; \forall t \in [t_{\min}, t_{\max}] \quad (4)$$

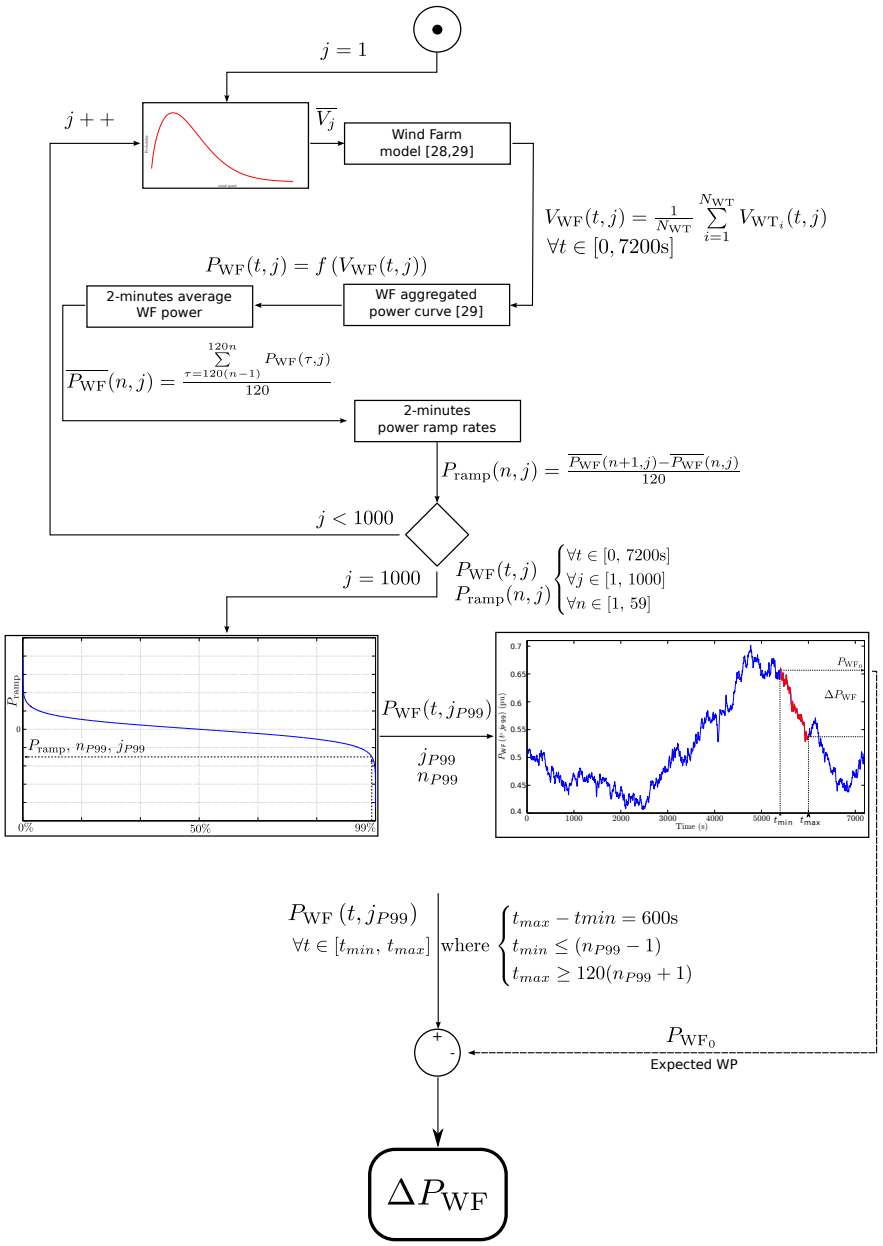

Figure 8. Sketch of the algorithm used for the simulation of critical wind power fluctuations.

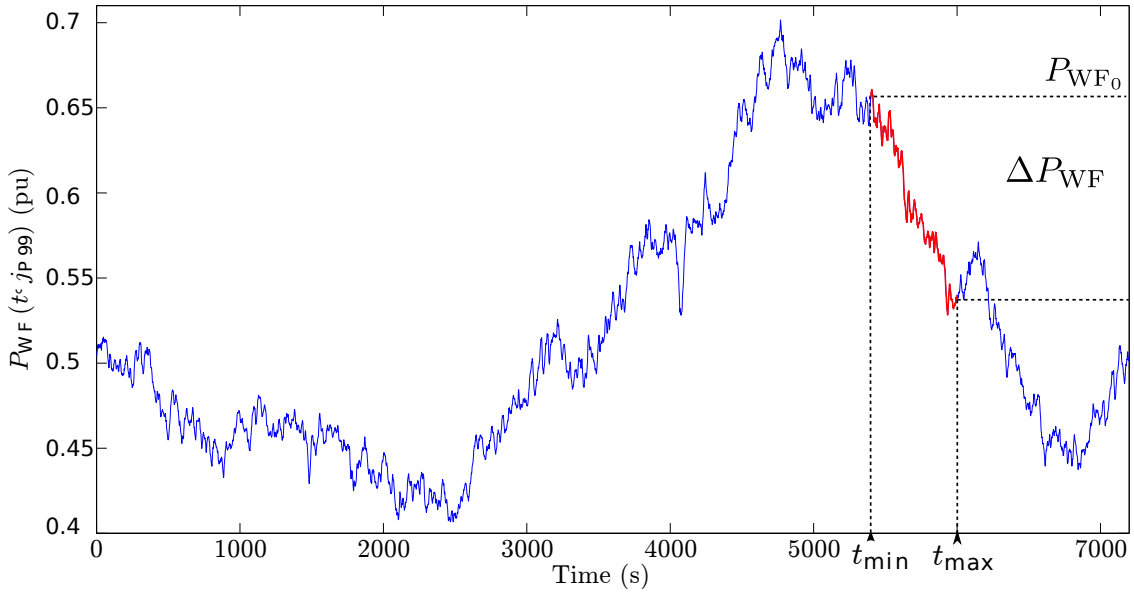

Figure 9. Wind farm power in 2-h time interval, expressed as per unit of installed wind power. In red, the 10-min interval used in the simulations.

4. Simulation and Results

4.1. Preliminaries

The simulated power system includes a thermal power plant and the previous wind farm. The parameters of the thermal power plant are shown in Table 1 based on [28]; see Figure 3.

Table 1. Parameters for the conventional generator model.

R_P	ΔP_{max}	$\dot{Y}_{max}$	$\dot{Y}_{min}$	α	T_{RH}	T_{CH}	H
5 %	0.05 pu	0.05 pu/s	−0.1 pu/s	0.3 pu	7 s	0.3 s	4 s

In order to reflect a low inertia in the modeled power system, the following assumptions are made: first, the contribution of the wind turbines to the system inertia is considered as negligible, since they are electrically decoupled from the grid; second, the inertia of the motor loads is also not considered. Therefore, it is assumed that the only inertial support comes from the thermal synchronous generator. An equivalent inertia constant (H_{eq}) can then be calculated by dividing the generator's kinetic energy at the rated speed by the system base power (S_b) as:

$$H_{eq} = \frac{\frac{1}{2}J_{th}\omega_0^2}{S_b} = \frac{\frac{1}{2}J_{th}\omega_0^2}{S_{th}}\frac{S_{th}}{S_b} = H\frac{S_{th}}{S_b} \tag{5}$$

J_{th} is the moment of inertia of the thermal generator, and ω_0 is its rated speed, so $\frac{1}{2}J_{th}\omega_0^2$ is the generator's kinetic energy at the rated speed. If the thermal plant relative size is chosen such that $\frac{S_{th}}{S_b} = \frac{3}{4}$, the equivalent inertia constant used for the simulations is $H_{eq} = 3$ s. For the damping coefficient (D' in Equation (1)) a typical value used in dynamic studies for isolated power systems, $D' = 1$, is chosen [28].

4.2. Implemented Scenarios

The worldwide residential sector accounts for about 30% of total electric energy consumption (TEEC) [21,38,39,41]. Considering two representative cases (winter and summer), the participation of

total residential electricity consumption (TREC) in the TEEC presents a maximum share of residential controllable loads of around 13% (30% · 43.0%) for the winter case and 10% (30% · 33.3%) for the summer case. Table 2 [21] shows the share of TREC by major end-use. For the sake of simplicity, a maximum share of residential controllable loads, in both the winter and summer cases, of 10% will be considered. For the proposed 1-GW power system model, 10% of the demand means 100,000 individual controllable loads.

Table 2. Share of residential electricity consumption by major end-use.

Group	Type of load	Share percentage (%)	
		Winter	*Summer*
I	Refrigeration and freezing	13.4	13.4
II	Space cooling	–	6.4
II	Space heating	16.1	–
III	Water heating	13.5	13.5
	Total	43.0	33.3

To evaluate the impact of demand-side participation on frequency control, a set of different scenarios are defined modifying the share of controllable loads. Specifically, 10-min time interval simulations are carried out for 2.5%, 5%, 7.5% and 10% of residential load share. In addition, and regarding the governor speed control for the supply side, different dead band values (20, 50, 80 and 100 mHz) are considered to give the demand side a more active role in frequency control. Subsequently, simulations for each governor's dead band are then compared to a reference case, in which demand-side response is not considered.

Finally, due to the presence of a certain degree of randomness in the load controller, simulations are repeated five times for each case study to include such variability.

4.3. Analysis of a Case Study: Winter Scenario

A detailed analysis of a specific case study is discussed in this subsection. A winter scenario is simulated considering 10% of controllable loads and a ±20-mHz governor's dead band.

Figure 10 depicts the corresponding frequency excursions and power deviations. To evaluate the demand response effect on frequency control, this figure also includes the $\Delta f(t)$ profile when demand side participation is not considered (blue line). As can be seen, there is a relevant reduction of oscillations in comparison with the reference case. Indeed, some of the peaks that surpass the upper bound are cut out, the frequency deviations within the thermal plant governor dead band being only dependent on the controllable load participation. Due to the very low system inertia, there are significant oscillations of the frequency around the limits of the thermal plant governor's dead band (20 mHz and −20 mHz). This effect of the inertia deficit on the grid stability was analyzed in a previous work [42].

Figure 10c shows the aggregated behavior of the controlled loads ($\Delta P^c_{L_f}$). It represents the forced load connection ($\Delta P^c_{L_f} > 0$) or disconnection ($\Delta P^c_{L_f} < 0$) with respect to their expected demand power profile. In this case study, the maximum positive power deviation is about 0.8% of the total demand, whereas the maximum negative power deviation is around 0.6%. The greater negative power deviations correspond to those time intervals where wind power drops steeply. Such time intervals are highlighted in Figure 10a. During these critical time intervals, the demand response contributes significantly to reducing the corresponding under-frequency excursions. In fact, the greater the ratio of controllable loads, the smoother the frequency deviations. To justify this assessment, Figure 11 compares frequency deviations for different controllable load ratios during the first critical time interval: $\forall t \in [5630, 5635]s$. In addition, Table 3 summarizes the reductions of the maximum under-frequency deviations for the different percentages of controllable loads.

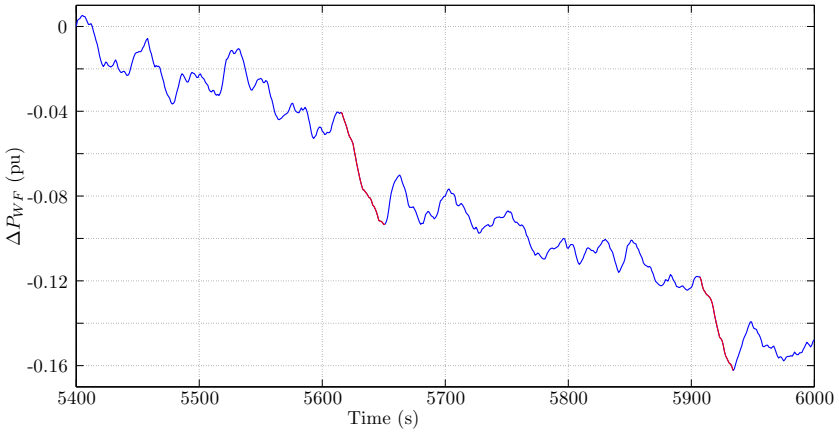

(a)

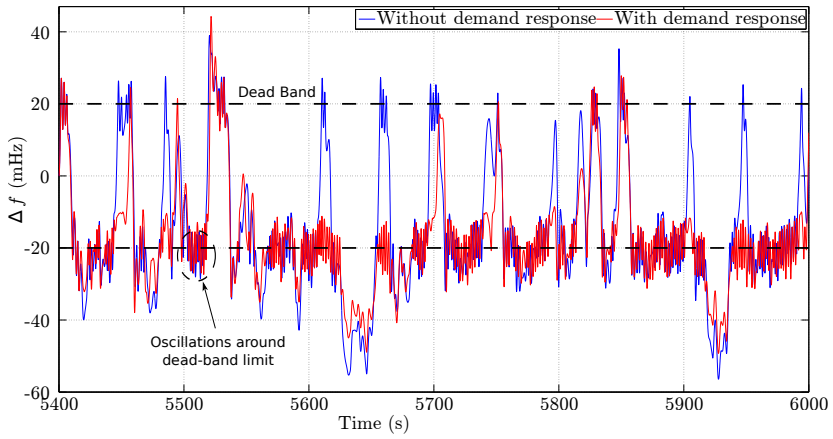

(b)

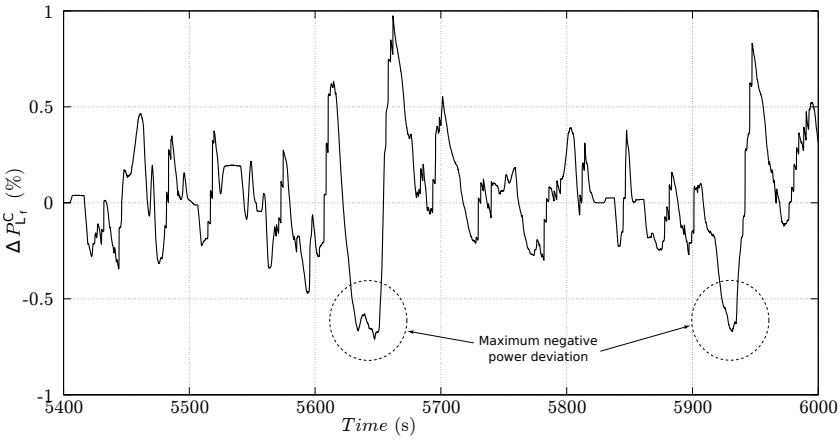

(c)

Figure 10. Results for a specific case study. (**a**) ΔP_{WF} for the most critical interval considered in the simulations; (**b**) example of the temporal evolution of frequency deviations when demand response is or not applied; (**c**) aggregated forced demand change.

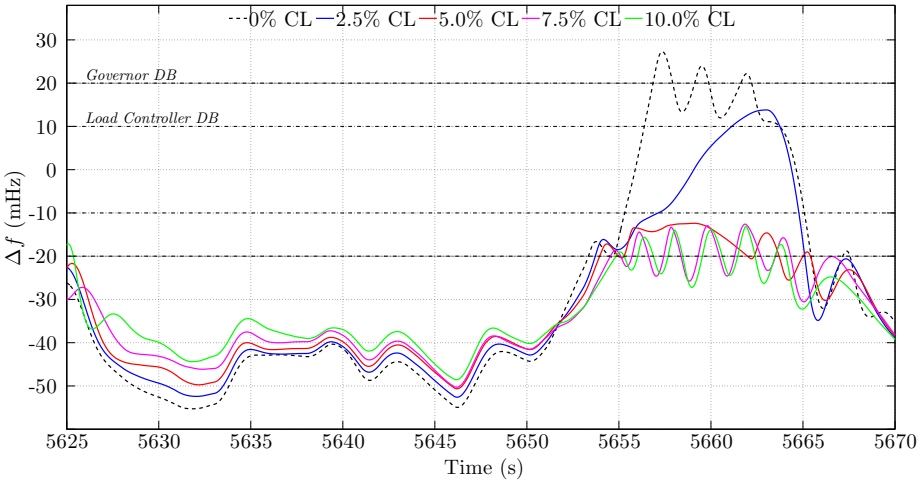

Figure 11. Δf for different percentages of controllable load, including the reference case.

Table 3. Δf_{min} variation (%) for $t \in [5630, 5635]$ s.

CL (%)	0	2.5	5	7.5	10
Winter	-	5.08	9.36	16.48	19.97
Summer	-	4.05	8.14	14.67	18.93

4.4. Summary of Case Studies

This subsection is devoted to providing an extensive analysis of the demand-response behavior for the set of winter and summer case studies.

In line with previously-observed results for the winter case, Figure 12 shows the increment in time during which frequency deviations are within the governor's dead band as a consequence of the controllable load actions. Such an increment is represented in percentages with respect to the uncontrolled reference case, according to Equation (6):

$$Improvement(\%) = \frac{T_{OK}^{C} - T_{OK}^{UC}}{T_{OK}^{UC}} \times 100 \tag{6}$$

being T_{OK}^{C} and T_{OK}^{UC} the total time during which $|\Delta f| < 20$ mHz with controlled and uncontrolled loads, respectively. For a given dead band, the growth of the time interval within the band is in general higher as the amount of controllable loads increases, *i.e.*, the higher the number of controllable loads, the lower the time in which the thermal generator's primary frequency controller remains active. For a $\pm$20-mHz dead band, both winter and summer cases, and also the winter case $\pm$100-mHz dead band, an increment of the controllable load rate from 7.5% to 10% does not lead to a significant improvement of the time interval within the dead band for the supply side. In fact, a certain saturation effect is detected in these cases.

In Figure 13, extreme deviations on power demand due to the individual load controllers are represented through both the 1- and 99-percentile of the power deviation with respect to the uncontrolled demand. Such deviations are given as per mille (‰) of the global demand, with relatively small demand modifications. Indeed, low values of Δf imply a reduced number of active controlled loads, enough remaining available controllable loads to provide a response under critical contingencies, as discussed by the authors in [25]. Controllable load thus significantly reduces the frequency excursion under large wind power fluctuations, keeping the capacity for the critical contingency response.

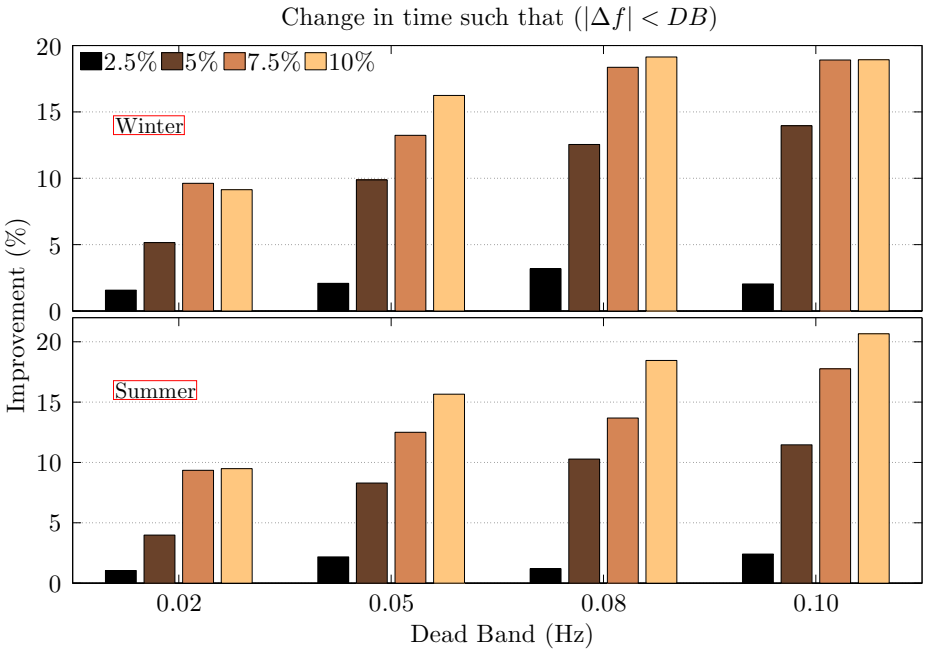

Figure 12. Increase of the time during which $|\Delta f| <$ dead band (DB) for different governor dead bands and controllable loads ; see Equation (6).

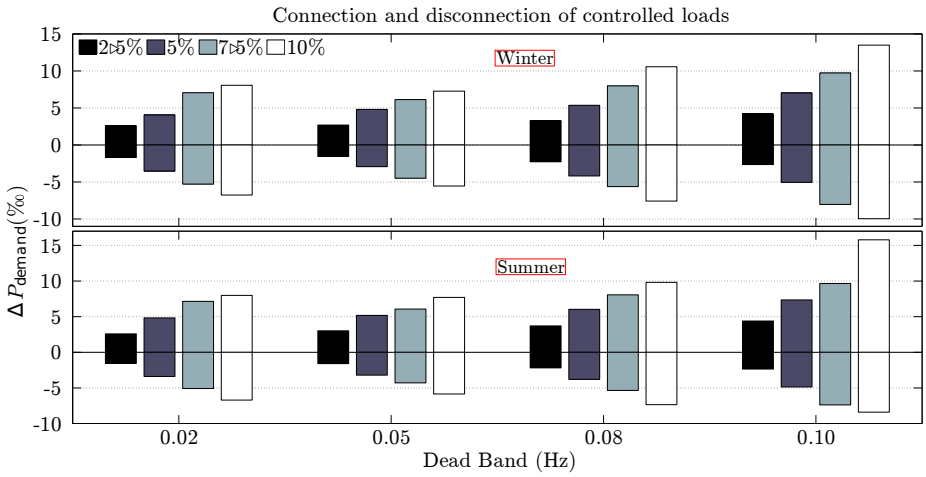

Figure 13. First and 99-percentiles (expressed in ‰) of connected or disconnected controlled loads for different governor dead bands and controllable loads.

5. Conclusions

A complete process to determine realistic wind oscillations is proposed to evaluate the contribution of the demand-side to primary frequency control in power systems with high wind penetration. These wind oscillations are determined based on a model for offshore wind power fluctuations, previously assessed through real data from the Nysted offshore wind farm. In this paper, extreme wind oscillations have been selected from 10,000 2-h series.

A steam turbine with conventional primary energy input control and an offshore wind farm are considered to model the supply side of a simplified power system. A highly fluctuating wind power data series is then used to emulate power system conditions. In particular, 10-min periods under the presence of negative and persistent ramps are selected as case studies. Primary and

secondary frequency control actions are only provided by the thermal power plant, evaluating different governor dead bands and controllable load levels.

The demand-side contribution to primary frequency control is considered using a decentralized approach not requiring any explicit communication. Thus, simple hardware can thermostatically control individual residential loads in response to deviations between the frequency and its nominal value over time. The behavior of different amounts of such controllers is simulated to study their effect at the system level when power fluctuations due to high wind energy penetration are considered. This high wind power penetration, when considering variable-speed wind turbines, implies that the system inertia can be critically low, resulting in high system instabilities.

Results show that it is possible to decrease primary frequency reserves with a relatively low demand-side participation in frequency control. Indeed, the time interval in which frequency deviations are within the governor's dead band is increased up to 20% with 10% of demand-side participation. Consequently, controllable loads significantly reduce frequency excursions under large power fluctuations, providing additional capacity for critical contingencies.

Acknowledgments: This work was supported by "Ministerio de Economía y Competitividad" and the European Union (ENE2012-34603), as well as by "*Fundación Séneca-Agencia de Tecnología de la Región de Murcia*" PCTIRM2011-14 (08747/PI/08 and 19379/PI/14).

Author Contributions: Jorge Villena developed and implemented the overall power system model, performed, analyzed and compared the simulations and prepared the manuscript. Antonio Vigueras-Rodríguez developed the original wind power generation model, proposed some simulation algorithms to evaluate the scenarios and provided comments on the manuscript. Emilio Gómez-Lázaro suggested several improvements on the analysis and comparisons of the simulation results and provided comments on the manuscript. Juan Álvaro Fuentes-Moreno prepared the conventional generation model and provided comments and suggestions on the manuscript. Irene Muñoz-Benavente implemented the supply-side model and helped with preparing the manuscript. Ángel Molina-García developed the supply-side model and provided comments on the results' comparison, as well as on the manuscript. All of the authors read and approved the final manuscript.

Conflicts of Interest: The authors declare no conflict of interest.

References

1. Weisser, D.; Garcia, R.S. Instantaneous wind energy penetration in isolated electricity grids: Concepts and review. *Renew. Energy* **2005**, *30*, 1299–1308.
2. Doherty, R.; Mullane, A.; Nolan, G.; Burke, D.; Bryson, A.; O'Malley, M. An assessment of the impact of wind generation on system frequency control. *IEEE Trans. Power Syst.* **2010**, *25*, 452–460.
3. Klempke, H.; McCulloch, C.; Wong, A.; Piekutowski, M.; Negnevitsky, M. Impact of high wind generation penetration on frequency control. In Proceedings of the 20th Australasian Universities Power Engineering Conference (AUPEC), Christchurch, New Zealand, 5–8 December 2010; pp. 1–6.
4. Gómez-Expósito, A.; Conejo, A.; Cañizares, C. *Electric Energy Systems: Analisys and Operation*; CRC Press: Boca Raton, FL, USA, 2009.
5. Fagan, E.; Grimes, S.; McArdle, J.; Smith, P.; Stronge, M. Grid code provisions for wind generators in Ireland. In Proceedings of the IEEE Power Engineering Society General Meeting, San Francisco, CA, USA, 12–16 June 2005; Volume 2, pp. 1241–1247.
6. Mullane, A.; O'Malley, M. The inertial response of induction-machine-based wind turbines. *IEEE Trans. Power Syst.* **2005**, *20*, 1496–1503.
7. Lalor, G.; Ritchie, J.; Rourke, S.; Flynn, D.; O'Malley, M.J. Dynamic frequency control with increasing wind generation. In Proceedings of the IEEE Power Engineering Society General Meeting, Denver, CO, USA, 6–10 June 2004; pp. 1715–1720.
8. Lalor, G.; Mullane, A.; O'Malley, M. Frequency control and wind turbine technologies. *IEEE Trans. Power Syst.* **2005**, *20*, 1905–1913.
9. Soerensen, P.; Hansen, A.D.; Thomsen, K.; Madsen, H.; Nielsen, H.A.; Poulsen, N.K.; Iov, F.; Blaabjerg, F.; Donovan, M.H. Wind farm controllers with grid support. In Proceedings of the 5th International Workshop on Large-Scale Integration of Wind Power and Transmission Networks for Offshore Wind Farms, Glasgow, UK, 7–8 April 2005.

10. Mokadem, M.E.; Courtecuisse, V.; Saudemont, C.; Robyns, B.; Deuse, J. Experimental study of variable speed wind generator contribution to primary frequency control. *Renew. Energy* **2009**, *34*, 833–844.
11. Morren, J.; de Haan, S.W.H.; Kling, W.L.; Ferreira, J.A. Wind turbines emulating inertia and supporting primary frequency control. *IEEE Trans. Power Syst.* **2006**, *21*, 433–434.
12. Bousseau, P.; Belhomme, R.; Monnot, E.; Laverdure, N.; Boeda, D.; Roye, D.; Bacha, S. Contribution of wind farms to ancillary services. In Proceedings of the Council on Large Electric Systems (CIGRE) General Meeting, Paris, France, 27 August–1 September 2006.
13. Yousefi, A.; Iu, H.C.; Fernando, T.; Trinh, H. An approach for wind power integration using demand side resources. *IEEE Trans. Sustain. Energy* **2013**, *4*, 917–924.
14. Concordia, C.; Fink, L.; Poullikkas, G. Load shedding on an isolated system. *IEEE Trans. Power Syst.* **1995**, *10*, 1467–1472.
15. Chuvychin, V.; Gurov, N.; Venkata, S.; Brown, R. An adaptive approach to load shedding and spinning reserve control during underfrequency conditions. *IEEE Trans. Power Syst.* **1996**, *11*, 1805–1810.
16. Cirio, D.; Demartini, G.; Massucco, S.; Morim, A.; Scalera, P.; Silvestro, F.; Vimercati, G. Load control for improving system security and economics. In Proceedings of the 2003 IEEE Bologna Power Tech Conference Proceedings, Bolgna, Italy, 23–26 June 2003; Volume 4, p. 8.
17. Delfino, B.; Massucco, S.; Morini, A.; Scalera, P.; Silvestro, F. Implementation and comparison of different under frequency load–shedding schemes. In Proceedings of the IEEE Power Engineering Society Summer Meeting, Vancouver, BC, Canada, 15–19 July 2001; Volume 1, pp. 307–312.
18. Zhao, Q.; Chen, C. Study on a system frequency response model for a large industrial area load shedding. *Int. J. Electr. Power Energy Syst.* **2005**, *27*, 233–237.
19. Vieira, J.; Freitas, W.; Wilsun, X.; Morelato, A. Efficient coordination of ROCOF and frequency relays for distributed generation protection by using the application region. *IEEE Trans. Power Deliv.* **2006**, *21*, 1878–1884.
20. Gu, W.; Liu, W.; Zhu, J.; Zhao, B.; Wu, Z.; Luo, Z.; Yu, J. Adaptive decentralized under-frequency load shedding for Islanded smart distribution networks. *IEEE Trans. Sustain. Energy* **2014**, *5*, 886–895.
21. International Energy Agency. *Cool Appliances: Policy Strategies for Energy-Efficient Homes*; Organization for Economic Co-operation and Development (OECD): Paris, France, 2003.
22. Bertoldi, P.; Atanasiu, B. *Electricity Consumption and Efficiency Trends in the Enlarged European Union*; Technical Report; European Commission – Institute for Environment Sustainability, 2007. Available online: http://ies.jrc.ec.europa.eu (accessed on 9 April 2011).
23. Malik, O.; Havel, P. Active demand-side management system to facilitate integration of RES in low-voltage distribution networks. *IEEE Trans. Sustain. Energy* **2014**, *5*, 673–681.
24. Short, J.A.; Infield, D.G.; Freris, L.L. Stabilization of grid frequency through dynamic demand control. *IEEE Trans. Power Syst.* **2007**, *22*, 1284–1293.
25. Molina-García, A.; Bouffard, F.; Kirschen, D. Decentralized demand-side contribution to primary frequency control. *IEEE Trans. Power Syst.* **2011**, *26*, 411–419.
26. Molina-García, A.; Muñoz Benavente, I.; Hansen, A.; Gómez-Lázaro, E. Demand-side contribution to primary frequency control with wind farm auxiliary control. *IEEE Trans. Power Syst.* **2014**, 29, 2391–2399.
27. Samarakoon, K.; Ekanayake, J. Demand side primary frequency response support through smart meter control. In Proceedings of the 44th International Universities Power Engineering Conference (UPEC), Glasgow, UK, 1–4 September 2009; pp. 1–5.
28. Kundur, P. *Power System Stability and Control*; McGraw-Hill: New York, NY, USA, 1994.
29. Ullah, N.R.; Thiringer, T.; Karlsson, D. Temporary primary frequency control support by variable speed wind turbines—Potential and applications. *IEEE Trans. Power Syst.* **2008**, *23*, 601–612.
30. REE. P.O. 7.1. *Servicio Complementario de Regulación Primaria*; Technical Report; Red Eléctrica de España: Madrid, Spain, 1998. Available online: http://www.ree.es (accessed on 20 May 2010).
31. UCTE. Operation Handbook – ver. 2.5. Technical Report; European Network of Transmission Network, Brussels, Belgium, 2004. Available online: https://www.entsoe.eu/resources/publications/system-operations/operation-handbook/ (accessed on 8 April, 2011).
32. Vigueras-Rodríguez, A.; Sørensen, P.; Cutululis, N.; Viedma, A.; Donovan, M. Wind model for low frequency power fluctuations in offshore wind farms. *Wind Energy* **2010**, *13*, 471–482.

33. Sørensen, P.; Hansen, A.D.; Carvalho-Rosas, P.E. Wind models for simulation of power fluctuations from wind farms. *J. Wind Eng. Ind. Aerodyn.* **2002**, *90*, 1381–1402.
34. Vigueras-Rodríguez, A. Modelling of the Power Fluctuations in Large Offshore Wind Farms. Ph.D. Thesis, Universidad Politécnica de Cartagena, Cartagena, Spain, 2008.
35. Sørensen, P.; Cutululis, N.; Vigueras-Rodríguez, A.; Madsen, H.; Pinson, P.; Jensen, L.; Hjerrild, J.; Donovan, M. Modelling of power fluctuations from large offshore wind farms. *Wind Energy* **2008**, *11*, 29–43.
36. Norgaard, P.; Holttinen, H. A multi-turbine power curve approach. In Proceedings of the Nordic Wind Power Conference (NWPC'04), Gothenburg, Sweden, 1–4 March 2004; Volume 1.
37. Wan, Y.; Ela, E.; Orwig, K. Development of an equivalent wind plant power curve. Proc. Wind Power, 2010, pp. 1–20.
38. Iain MacLeay, K.H.; Annut, A. *Digest of United Kingdom Energy Statistics 2014*; National Statistics Publication: London, UK, 2014.
39. International Energy Agency (IEA). *World Energy Outlook* 2014. Technical Report; IEA: Paris, France, 2014. Available online: http://dx.doi.org/10.1787/weo-2014-en (accessed on 14 July 2015).
40. Vigueras-Rodríguez, A.; Sørensen, P.; Viedma, A.; Donovan, M.H.; Gómez-Lázaro, E. Spectral coherence model for power fluctuations in a wind farm. *J. Wind Eng. Ind. Aerodyn.* **2012**, *102*, 14–21.
41. Saidur, R.; Masjuki, H.H.; Jamaluddin, M.Y. An application of energy and exergy analysis in residential sector of Malaysia. *Energy Policy* **2007**, *35*, 1050–1063.
42. Villena-Lapaz, J.; Vigueras-Rodríguez, A.; Gómez-Lázaro, E.; Molina-García, A.; Fuentes-Moreno, J.A. Stability assessment of isolated power systems with high wind power penetration. In Proceedings of the European Wind Energy Asociation Conference (EWEA), Copenhagen, Denmark, 16–19 April 2012.